Shear viscosity of strongly coupled Yukawa liquids

Z. Donkó and P. Hartmann
Research Institute for Solid State Physics and Optics of the Hungarian Academy of Sciences, H-1525 Budapest, P.O. Box 49, Hungary
(Received 10 June 2008; published 19 August 2008)

We present molecular-dynamics calculations of the shear viscosity of three-dimensional strongly coupled Yukawa liquids which are frequently used as a model system of complex plasmas. The results obtained using two independent nonequilibrium simulation methods are critically compared with each other and with earlier published data for a wide range of plasma coupling (Γ) and screening (κ) parameters. The non-Newtonian behavior of the liquid, manifested as a descrease of the shear viscosity with increasing shear rate (shear thinning), and the validity of the Stokes-Einstein relation at high coupling strength are also demonstrated.

DOI: 10.1103/PhysRevE.78.026408 PACS number(s): 52.27.Gr, 52.25.Fi, 52.27.Lw

I. INTRODUCTION

Strongly coupled plasmas—in which the average potential energy per particle dominates over the average kinetic energy—appear in a wide variety of physical systems [1]. Many of these systems share some properties, which allows one to describe them by the "one-component plasma" (OCP) model. This model considers explicitly only a single type of charged particles and uses a potential that accounts for the presence and effects of other types of species. The latter may be considered as a charge-neutralizing background, which is either nonpolarizable or polarizable. In the case of a polarizable background, the screening property of the plasma is expressed by the Yukawa potential

$$\phi(r) = \frac{Q}{4\pi\varepsilon_0}\frac{\exp(-r/\lambda_D)}{r}, \tag{1}$$

where Q is the particle charge and λ_D is the Debye length. Examples of systems lending themselves to the approximation of the interaction by the Yukawa potential include dusty plasmas [2–6] and charged colloids [7–10].

Yukawa one-component plasmas ("YOCP") are fully characterized by the *coupling parameter*,

$$\Gamma = \frac{Q^2}{4\pi\varepsilon_0}\frac{1}{ak_BT}, \tag{2}$$

and the *screening parameter*,

$$\kappa = \frac{a}{\lambda_D}, \tag{3}$$

where $a=(3/4\pi n)^{1/3}$ is the Wigner-Seitz (WS) radius, n is the particle number density, and T is the temperature. At $\kappa\to 0$, the Coulomb OCP is recovered.

In the case of the Coulomb OCP, strong coupling corresponds to $\Gamma \gg 1$. In this domain, the OCP exhibits properties of a liquid [11] until, at $\Gamma_m \approx 175$, a liquid$\to$solid phase transition occurs [12]. Γ_m is known to increase with increasing κ [13].

Transport coefficients of the strongly coupled OCP and YOCP liquids have attracted considerable interest during the past decades. The shear viscosity η has an effect on, e.g., the hydrodynamic behavior of these systems and on wave propagation. It is defined by the constitutive relation

$$j_y = -\eta\frac{dv_x(y)}{dy}, \tag{4}$$

which relates a momentum flux j_y to the velocity gradient $dv_x(y)/dy$, also termed the shear rate (γ).

Data available in the literature for the Coulomb OCP shear viscosity, as a function of Γ, are reviewed in Fig. 1(a). The data are given in reduced (dimensionless) units $\eta' = \eta/mn\omega_p a^2$, where $\omega_p=\sqrt{nQ^2/\varepsilon_0 m}$ is the plasma frequency and m is the mass of the particles. Early calculations for η of the Coulomb OCP were carried out (in the 1970s) by Vieillefosse and Hansen [14] from the current correlation functions of the plasma. A prominent feature of the $\eta(\Gamma)$ curve is the minimum occurring at intermediate coupling $\Gamma\approx 20$, which is due to the prevailing kinetic and potential contributions of the viscosity at low and high coupling, respectively (see, e.g., [15]). Wallenborn and Baus [16] obtained their viscosity data from the kinetic theory of the OCP. Molecular-dynamics (MD) simulation for the calculation of the OCP shear viscosity was applied by Bernu, Vieillefosse, and Hansen [17]. Their values agree quite well with those obtained from more recent MD simulations of Donkó and Nyíri [18], and of Bastea [19], as can be seen in Fig. 1(a). The data obtained from YOCP simulations of Salin and Caillol [20] and Saigo and Hamaguchi [15] in the limit of small screening (κ) also confirm these Coulomb OCP molecular-dynamics results.

For Yukawa liquids, results for the shear viscosity have appeared only during the past decade. Data available in the literature, taking as an example the $\kappa=2$ case, are displayed in Fig. 1(b). Besides the normalization leading to η' (see above), for Yukawa systems we also use the normalization by the Einstein frequency ω_E, yielding $\eta^*=\eta/mn\sqrt{3}\omega_E a^2$. The use of the Einstein frequency (the oscillation frequency of a test charge in the frozen environment of the particles of the system) has been pointed out to be more appropriate for Yukawa systems, as ω_E depends on the screening parameter κ. Note then that at $\kappa=0$, we have $\eta'=\eta^*$ as $\omega_p=\omega_E\sqrt{3}$ (see, e.g., [21]).

The calculations of Murillo [22] and Faussurier and Murillo [23] plotted in Fig. 1(b) have been based on, respec-

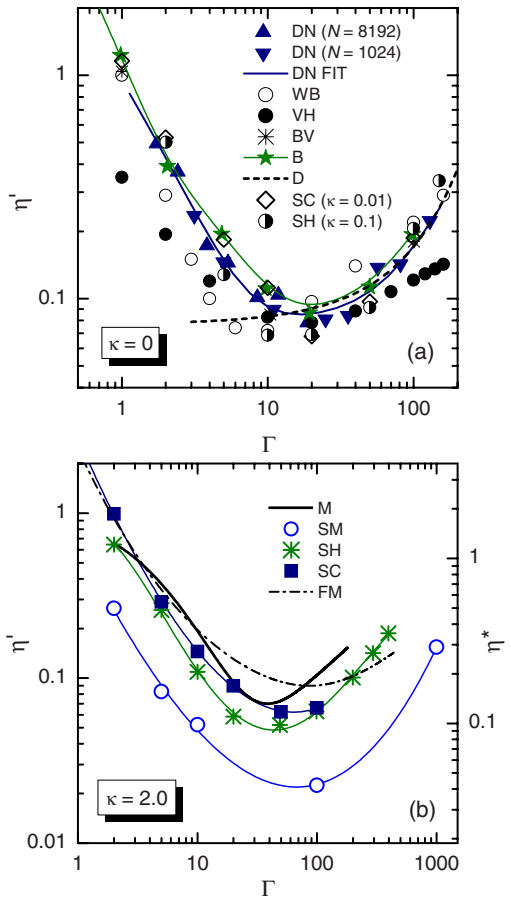

FIG. 1. (Color online) (a) Shear viscosity of the Coulomb OCP. DN: Donkó and Nyíri [18] using 1024 and 8192 particles; WB: Wallenborn and Baus [16]; VH: Vieillefosse and Hansen [14]; BV: Bernu *et al.* [17]; B: Bastea [19]. The dashed line (D: Daligault [11]) represents an Arrhenius-type behavior at high Γ values; this curve has been scaled to match the minimum value of η. Additional data for YOCP with small screening coefficent: SC: Salin and Caillol [20]; SH: Saigo and Hamaguchi [15]. (b) Shear viscosity of the Yukawa OCP at κ=2. M: Murillo [22]; SM: Sanbonmatsu and Murillo [24]; FM: viscosity obtained from mapping with effective hard-sphere system by Faussurier and Murillo [23]; SC and SH: see (a).

tively, mapping between the Yukawa system and the Coulomb, as well as hard-sphere systems. Sanbonmatsu and Murillo [24] applied nonequilibrium MD simulation for the determination of η, while the most recent studies [15,20] utilized equilibrium MD simulations. (The details of these approaches are presented in Sec. II.) As compared to the Coulomb case, the coupling value (Γ), where the minimum of η occurs, is shifted toward higher values, and some of the data indicate that the minimum value of η is decreased.

Figure 1(b) shows a significant discrepancy between the results of the independent calculations of η. Although the η versus Γ curves show the same general features, there is a factor of 5 difference regarding the minimum value of the viscosity $\eta_{\min}$ and a factor of 3 difference regarding the position of the minimum $\Gamma_{\min}$. Considering only the most recent simulation data sets of Saigo and Hamaguchi [15] and Salin and Caillol [20], we find much less scattering of the data, nevertheless, e.g., at Γ=20, a difference of about 50% between the η values still exists.

In view of these discrepancies, more accurate determination of the shear viscosity of Yukawa liquids is desirable, and this is indeed the motivation of the present work. As the Yukawa system is also used as a reference for calculations of viscosity of systems like liquid metals and warm dense matter through mapping of these systems with the Yukawa model [25], obtaining more accurate data for η would clearly be important. Here we apply two different MD simulation approaches to obtain viscosity values and compare the results of these calculations with each other and also with the earlier data of the above-mentioned authors.

Additionally, we demonstrate the non-Newtonian behavior of the 3D Yukawa liquids, manifested as the change of the viscosity with increasing shear rate. Such behavior has previously been found in experimental studies of complex plasmas [26,27] and in simulations of a two-dimensional Yukawa liquid [28].

We also examine the validity of the Stokes-Einstein relation, which establishes a connection between the shear viscosity and the self-diffusion coefficient D as $D\eta/T \cong$ const [29]. Simulation studies to test the validity of this relation for 2D Yukawa liquids have been carried out by Liu *et al.* [30] and for 3D one-component Coulomb liquids by Daligault [11]. For 3D Yukawa liquids, experimental investigations have been presented by Vaulina *et al.* [31]. In the 2D case, the Stokes-Einstein relation was found to be valid for a narrow range of parameters, due to the superdiffusive behavior of the system outside this range. Numerical studies on quasi-2D dissipative Yukawa systems indicated that the Stokes-Einsten relation holds for a wide domain in the strongly coupled regime [32]. For 3D Coulomb liquids, the relation was found to be fulfilled for a wide range of conditions; significant deviation was found to occur only at lower coupling values ($\Gamma \lesssim 20$) [11].

Section II of the paper describes different simulation techniques, which can be used for the determination of the shear viscosity. Section III presents the results obtained using two of these methods, and compares the present results with earlier published data. The shear thinning effect and the validity of the Stokes-Einstein relation is also discussed here. The work is summarized in Sec. IV.

II. SIMULATION METHODS FOR THE CALCULATION OF SHEAR VISCOSITY

Molecular-dynamics simulations, in general, offer two basic approaches for the determination of transport coefficients. In *equilibrium* simulations, correlation functions of certain microscopic quantities are measured and the transport coefficients are determined from the Green-Kubo relations. In *nonequilibrium* simulations, a perturbation is applied to the system and the response—linked with the perturbation via a transport coefficient—is measured. In the following, we present some of the methods (one equilibrium and three nonequilibrium techniques) that have been applied previously for the calculation of the shear viscosity in many-particle

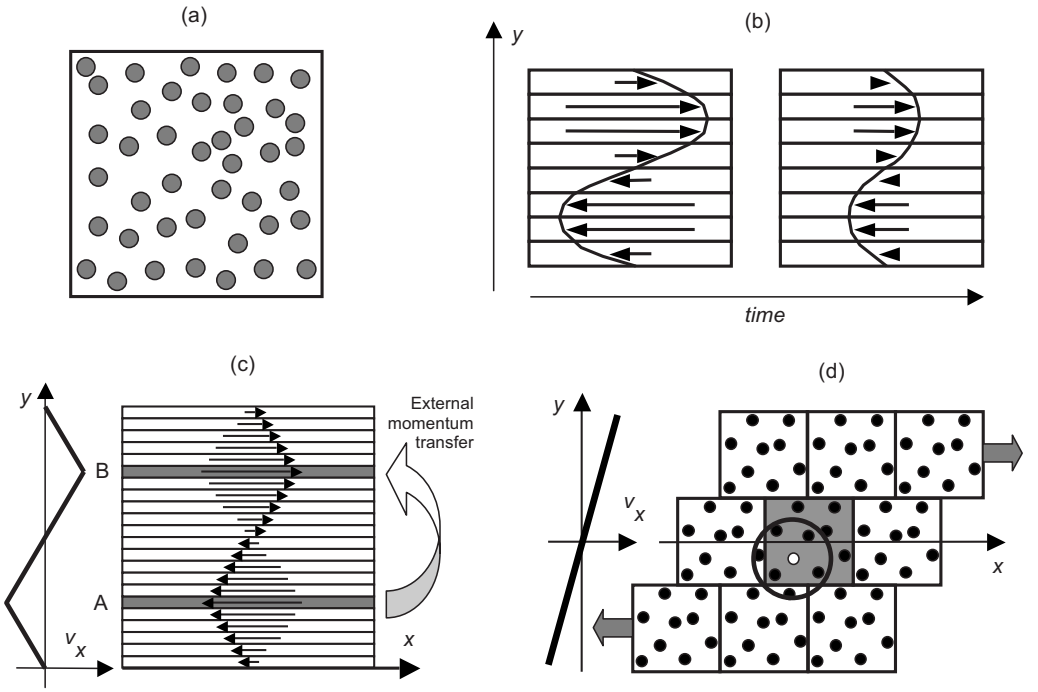

FIG. 2. Simulation methods for shear viscosity calculation. (a) Equilibrium MD: uses phase-space trajectories to compute η. (b) Transient perturbation technique: the decay time of an artificial velocity profile modulation is monitored. (c) Reverse molecular dynamics: an exchange of particles' momenta between cells A and B results in a velocity profile. (d) Homogeneous shear algorithm using sliding periodic boundary conditions. The figures show 2D faces of the 3D computational boxes. For more details about the different methods, see text.

simulations; see Fig. 2. Two of the nonequilibrium approaches serve the basis of our calculations presented here.

A. Equilibrium MD simulation

In this approach [Fig. 2(a)], the time-dependent phase-space trajectories of the particles (obtained in the MD simulation) are used to compute the off-diagonal element of the pressure tensor,

$$P^{xy} = \sum_{i=1}^{N} \left[m v_{ix} v_{iy} - \frac{1}{2} \sum_{j \neq i}^{N} \frac{x_{ij} y_{ij}}{r_{ij}} \frac{\partial \phi(r_{ij})}{\partial r_{ij}} \right], \tag{5}$$

where N is the number of particles, and $r_{ij} = |\mathbf{r}_{ij}| = |\mathbf{r}_i - \mathbf{r}_j| = |(x_{ij}, y_{ij})|$. The shear viscosity coefficient may be determined from the Green-Kubo integral [33],

$$\eta = \frac{1}{VkT} \int_0^\infty \langle P^{xy}(t) P^{xy}(0) \rangle \mathrm{d}t, \tag{6}$$

where $C_\eta = \langle P^{xy}(t) P^{xy}(0) \rangle$ is the stress autocorrelation function (SACF). The simulation uses periodic boundary conditions [also the ones presented subsequently, although this is explicitly shown only in Fig. 2(d)].

B. Transient perturbation method

This method, illustrated in Fig. 2(b), is based on the monitoring of the relaxation of the spatial velocity profile following a perturbation of the system [18], which can be given as

$$W(y_k) = W_{M0} \sin\left(\frac{2\pi y_k}{L} \right), \tag{7}$$

where $W = \langle v_{xi} \rangle_{i=1,\ldots,N}$, v_{xi} is the x velocity component of the ith particle, W_{M0} is the amplitude of the velocity modulation, and y_k are the coordinates of the slabs into which the simulation box (of edge length L) is partitioned [see Fig. 2(b)]. Note that the average "x" velocity $\langle v_x \rangle$ is zero before the modulation, except of some statistical noise of the simulation. After this "initial" modulation, the $W(x,t)$ velocity profile is measured at each time step, a sinusoidal function is fitted to it, and its harmonic amplitude $W_M(t)$ is determined. The amplitude is expected to fall exponentially, according to the

$$W(y,t) = W_{M0} \sin\left(\frac{2\pi y}{L} \right) \exp\left(-\frac{t - t_0}{\tau} \right) \tag{8}$$

solution of the equation for shear viscosity,

$$\frac{\partial v_x}{\partial t} = \frac{\eta}{\rho} \frac{\partial^2 v_x}{\partial y^2}, \tag{9}$$

where τ is the characteristic time of the relaxation and ρ is the mass density. Having measured τ, the shear viscosity is determined as [18]

$$\eta = \frac{\rho}{\tau} \left(\frac{L}{2\pi} \right)^2. \tag{10}$$

C. Reverse molecular dynamics

In this technique (introduced by Müller-Plathe [34]), the cause-and-effect picture usually used in nonequilibrium molecular dynamics is reversed: the effect, the momentum flux, is imposed, and the cause, the velocity gradient (shear rate), is measured in the simulation. The momentum in the liquid is introduced in a pair of narrow slabs A and B [see Fig. 2(c)], which are situated at $y=L_y/4$ and $3L_y/4$, respectively (L_y is the edge length of the simulation box in the y direction). At regular time intervals τ, we identify the particles in slabs A and B having the highest $|v_x|$ in the positive and negative directions, respectively. We then instantaneously exchange the v_x velocity component of these two particles without moving the particles themselves. This artificial transfer of momentum between slabs A and B (which is accomplished without changing the system energy) creates a velocity profile $v_x(y)$ throughout the system, the slope of which can be controlled by the frequency of the momentum exchange steps.

One can obtain η from

$$\eta \frac{dv_x(y)}{dy} = \frac{\Delta p}{2t_{\mathrm{sim}}S}, \tag{11}$$

where Δp is the total x-directional momentum exchanged between slabs A and B during the whole simulation time t_{sim}, and S is the area of the simulation box perpendicular to the y direction [34] [see Fig. 2(c)].

D. Homogeneous shear algorithm

The homogeneous shear algorithm of Evans and Morriss [35] simulates a planar Couette flow, which builds up in the system as a consequence of using the Lees-Edwards (sliding) periodic boundary conditions, as shown in Fig. 2(d). One obtains a homogeneous streaming flow field in the simulation box: $\langle v_x \rangle = \gamma(y - L_y/2)$, where $\langle\ \rangle$ denotes time average and γ is the shear rate. The system is described by the Gaussian thermostatted SLLOD equations of motion (see [35]),

$$\frac{d\mathbf{r}_i}{dt} = \frac{p_i}{m} + \gamma y_i \hat{\mathbf{x}},$$

$$\frac{d\tilde{\mathbf{p}}_i}{dt} = \mathbf{F}_i - \gamma \tilde{p}_{yi}\hat{\mathbf{x}} - \alpha p_i, \tag{12}$$

where $p=(\tilde{p}_x,\tilde{p}_y)$ is the *peculiar* momentum of particles, x is the unit vector in the x direction, and α is the Gaussian thermostatting multiplier. The above set of equations is solved using an operator splitting technique [36]. The shear viscosity is obtained as

$$\eta = -\lim_{t\to\infty} \frac{\langle P^{xy}(t)\rangle}{\gamma}, \tag{13}$$

where P^{xy} is defined by Eq. (5).

III. RESULTS AND DISCUSSION

For the calculation of transport coefficients, nonequilibrium methods are generally more efficient than equilibrium calculations. Moreover, in the latter approach, difficulties with the calculation of the integral (6) may arise due to the not well known long-time behavior (possibly algebraic decay) of the correlation function C_λ. Thus our choice for the calculation of the shear viscosity of 3D strongly coupled Yukawa liquids is to apply nonequilibrium simulations; from the methods presented above, we use the techniques in which the systems reach quasistationary perturbed states: (i) the reverse molecular-dynamics method (Sec. II C) and (ii) the homogeneous shear algorithm (Sec. II D). We refer to these techniques as "RMD" and "HSA" in the rest of the paper. We apply periodic boundary conditions to the simulation box. The number of particles is set between 1000 and 64 000, which allows a study of the effect of system size. Pairwise Yukawa interparticle forces are summed over a κ-dependent cutoff radius (also extending into the periodic images of the primary computational cell), using the chaining mesh technique [37].

In the case of the RMD method, no thermostat is used; the desired system temperature is set by rescaling the momenta of the particles in the initialization phase of the simulation that precedes the start of data collection. The amplitude of the velocity profile that establishes in the system depends on the frequency of momentum exchange steps. This way arbitrarily small velocity gradients can be established, causing very small perturbation to the system. However, at very low $dv_x(y)/dy$ noise may be dominant, thus a proper choice of the delay between momenta exchanges is a compromise between the degree of perturbation and the signal-to-noise ratio of the quantities [$dv_x(y)/dy$ and Δp, see Eq. (11)] to be measured. We have obtained our results at $[dv_x(y)/dy](L/2v_0) \sim 0.2-0.3$. Here $v_0=(2k_BT/m)^{1/2}$ is the average thermal velocity of the particles. The $v_x(y)$ velocity profiles have been found to be nearly linear for most of our conditions, except at the lowest values of Γ, indicating a longer equilibration distance, which is no longer negligible compared to simulation box size [38].

When using the HSA, different values for the normalized shear rate $\bar{\gamma}=(dv_x/dy)(a/v_0)$ are used. For 2D settings, a decrease of the viscosity with increasing $\bar{\gamma}$ was found to occur; a similar shear thinning effect is also expected to occur in 3D. Thus, while we aim to use as low as possible $\bar{\gamma}$ to obtain the "near-equilibrium" shear viscosity, we also examine the effect of higher values of $\bar{\gamma}$ on the viscosity.

The chief results of our calculations are presented in Figs. 3–5, respectively, for $\kappa=1$, 2, and 3. Panels (a) of the figures show our results obtained with the homogeneous shear algorithm using $N=8000$ particles at a normalized shear rate of $\bar{\gamma}=0.05$, as well as the previous data taken from the works of Sanbonmatsu and Murillo [24], Saigo and Hamaguchi [15], and Salin and Caillol [20]. The shear rate $\bar{\gamma}=0.05$ for the determination of the "near-equilibrium" values of the viscosity has been chosen as a compromise: at this value, the viscosity is expected to remain close to its equilibrium value and the signal-to-noise ratio of the measured $P^{xy}(t)$ [see Eq. (13)] is still acceptable, unlike at $\bar{\gamma} \lesssim 0.02$.

Panels (b) of Figs. 3–5 compare the results obtained here by using the two different techniques, different system sizes, and shear rates via normalizing the data with a reference set of data. This latter is chosen to be the results of the homo-

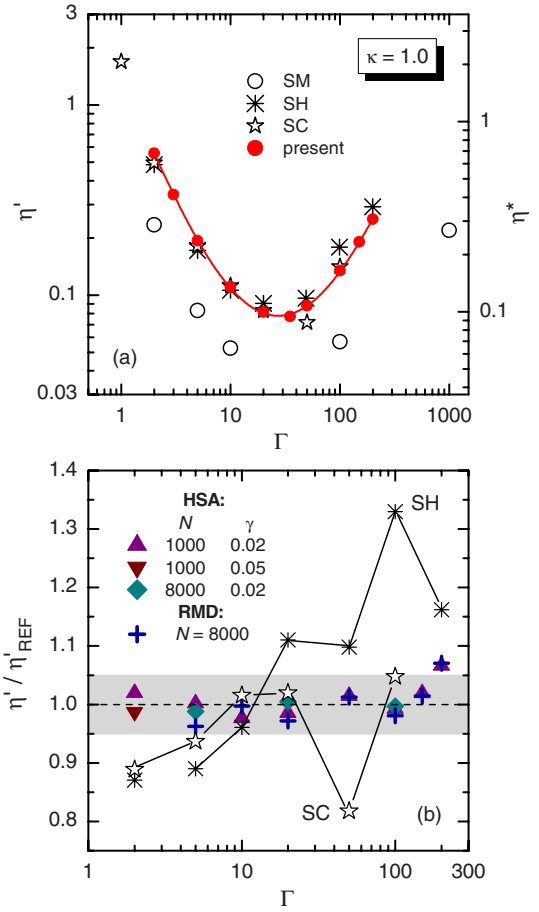

FIG. 3. (Color online) (a) Shear viscosity of the Yukawa liquid at $\kappa=1$. SM: Sanbonmatsu and Murillo [24]; SH: Saigo and Hamaguchi [15]; SC: Salin and Caillol [20]; present: results obtained with the homogeneous shear algorithm (HSA) using $N=8000$ particles and a normalized shear rate $\bar{\gamma}=0.05$. Left scale: viscosity values normalized by the plasma frequency (η'); right scale: viscosity values normalized by the Einstein frequency (η^*). (b) Comparison of the results obtained by using different methods in the present work [HSA: homogeneous shear algorithm, with number of particles (N) and at reduced shear rates ($\bar{\gamma}$) indicated; RMD: reverse molecular dynamics with number of particles (N) indicated] and with viscosity values obtained in previous works (SH and SC, see above). The present data shown in (a) have been taken as reference data, η'_{REF}. The shaded region represents $\pm 5\%$ deviation from the reference data.

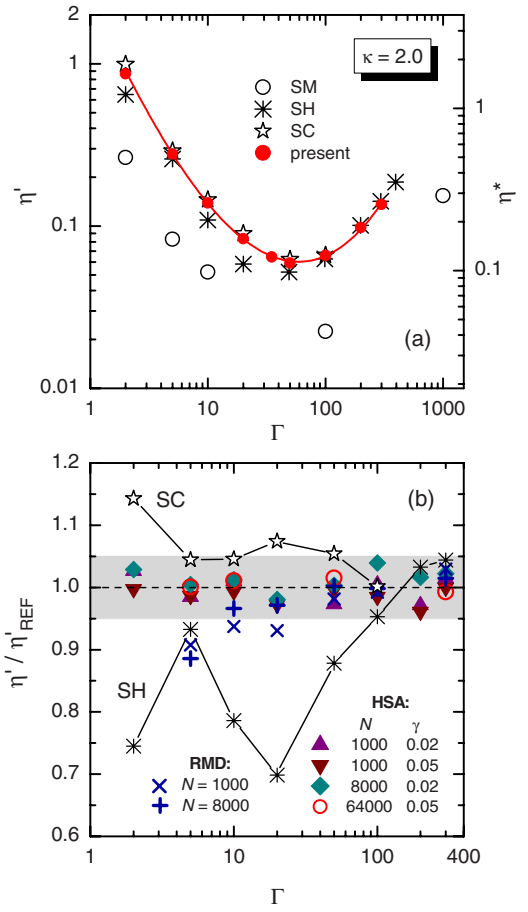

FIG. 4. (Color online) Shear viscosity of the Yukawa liquid at $\kappa=2$. For details, see the caption of Fig. 3.

geneous shear algorithm, at $N=8000$ and $\bar{\gamma}=0.05$ [i.e., the data shown in panels (a)]. In addition to the present data, the earlier viscosity values derived by Saigo and Hamaguchi [15] as well as by Salin and Caillol [20] (referenced as "SH" and "SC" data, respectively, in the sequel) are also shown for comparison. As mentioned earlier, these are the two previous sets of data that are the closest to the present values.

We start with the analysis of the $\kappa=1$ case. For this case, see Fig. 3(a), the SH and SC data agree well with each other at lower coupling ($\Gamma \lesssim 30$) values but at higher coupling SH predict higher viscosity. The data of Ref. [24] are about a factor of 2 too low, compared to the SH and SC data. The results of the present calculations lie close to the SH and SC data at lower Γ but are definitely lower than the SH data at high Γ. More details about the agreement between the different data sets are revealed in Fig. 3(b). For $\kappa=1$, we have carried out five different simulations: we used the homogeneous shear algorithm (HSA) with $N=1000$ and 8000 particles, and with $\bar{\gamma}=0.02$ and 0.05 shear rates (four cases) and the reverse MD method (RMD) with $N=8000$ particles. We take the HSA results with $N=8000$ and $\bar{\gamma}=0.05$ as reference (as explained above) and show the results of the "other" simulations normalized by these data. Also normalized by these present data are the SH and SC data shown in Fig. 3(b). One can notice that at some of the Γ values, there is up to 30% difference between the SH and SC data. The differences between the present data sets (obtained in the different simulations) are, on the other hand, much smaller. Most of the data points fall within a $\pm 5\%$ range around the reference data, regardless of the method used (HSA versus RMD) and the parameter (system size and shear rate) settings in the HSA method.

An even more detailed comparison between the different simulations is carried out for $\kappa=2$ (see Fig. 4). For this case, we have extended the system size in the HSA up to $N=64\,000$ particles, and we have carried out RMD simulations with two system sizes ($N=1000$ and 8000), as well. These, together with the reference set of data, give seven different parameter combinations. As one can see in Fig. 4(b), all the data except some of the RMD results at lower Γ values lie

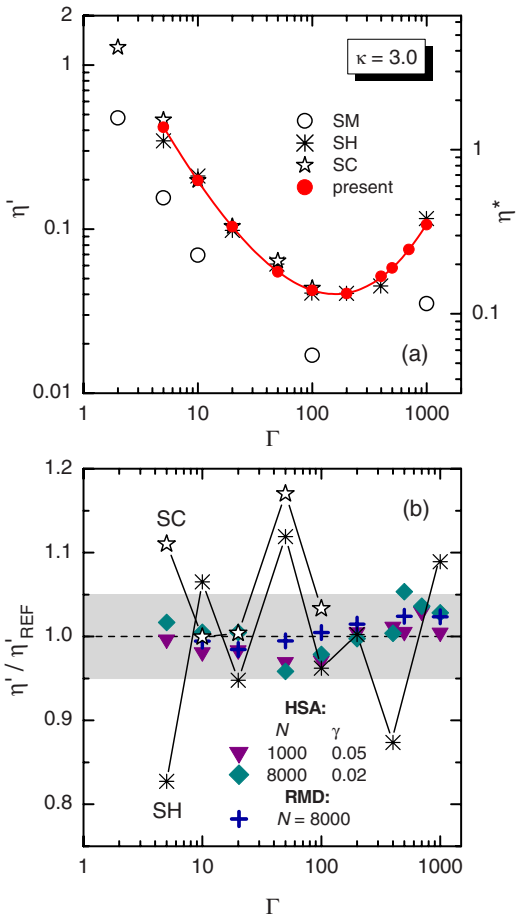

FIG. 5. (Color online) Shear viscosity of the Yukawa liquid at $\kappa=3$. For details, see the caption of Fig. 3.

within a $\pm 5\%$ range around the reference data. It is rather remarkable that the HSA gives data in close agreement with each other over the wide range of system sizes, from $N=1000$ to 64 000. This implies that this method is rather accurate even in the case of small system sizes. As regards the RMD data, the agreement with the HSA results is good at high coupling. In this range, we observed rather linear $dv_x(y)/dy$ profiles. The profiles, however, became more peaked at the positions of momentum exchange (slabs A and B, see Sec. II C) at lower Γ. This behavior may originate from an increasing equilibration distance with decreasing Γ, and results in a deviation of the results from the reference data. Note that the deviation shows up earlier (when decreasing Γ) in the case of the smaller ($N=1000$ particle) system. These observations confirm that one can expect accurate results from the RMD method only as long as the particle equilibration distance is much shorter than the edge length of the simulation box.

The $\kappa=3$ case is analyzed in Fig. 5. Here we compare four simulation data sets. Again, the agreement between the HSA and RMD results is very good; the data fall within the $\pm 5\%$ range around the reference data, except one of the data points. The scattering of the data is significantly lower compared to the SH and SC data.

The reproducibility of the simulation results was tested at $\kappa=2$ for $\Gamma=10$ and 200. For each of these cases, six HSA simulation runs have been carried out with $N=8000$ particles, at a normalized shear rate of $\bar{\gamma}=0.05$. The error of the results (3σ) proved to be 1.2% for $\Gamma=10$ and 1.6% for $\Gamma=200$. While we were not able to carry out such a test for the whole range of Γ and κ values covered in our study, we expect that our values have an accuracy better than 5% over the whole domain of the parameters. This accuracy looks to be far better than that of any previous data sets, as seen in panels (b) of Figs. 3–5. The values used as reference data in these figures are listed in Table I.

TABLE I. Shear viscosity of 3D Yukawa liquids normalized by the plasma frequency (η') and by the Einstein frequency (η^*). Results of the homogeneous shear algorithm (HSA) using $N=8000$ particles and a reduced shear rate $\bar{\gamma}=0.05$.

	η'			η^*		
Γ	$\kappa=1$	$\kappa=2$	$\kappa=3$	$\kappa=1$	$\kappa=2$	$\kappa=3$
2	0.558			0.682		
3	0.338			0.413		
5	0.193	0.278	0.417	0.236	0.523	1.369
10	0.110	0.139	0.198	0.135	0.261	0.650
20	0.0814	0.0836	0.104	0.0995	0.157	0.340
35	0.0773	0.0644		0.0945	0.121	
50	0.0878	0.0592	0.0548	0.107	0.111	0.180
100	0.135	0.0659	0.0423	0.165	0.124	0.139
150	0.190			0.233		
200	0.251	0.0978	0.0405	0.307	0.184	0.133
300		0.136			0.256	
400			0.0515			0.169
500			0.0579			0.190
700			0.0752			0.247
1000			0.107			0.350

The non-Newtonian behavior of 2D Yukawa liquids has been studied previously [28]. Here we illustrate similar behavior of the 3D liquid, however a thorough analysis and parametric study of the effect is beyond the scope of the present paper.

The dependence of the shear viscosity on the shear rate is studied at $\kappa=2$, for $\Gamma=10$, 50, and 300. The shear rate $\bar{\gamma}$ is varied here between 0.02 and 1.0. The results of the calculations are presented in Fig. 6(a). At $\bar{\gamma}\to 0$, the viscosity is nearly equal for $\Gamma=10$ and 300. Also at both of these Γ values, we observe an approximately factor of 2 decay of η as the shear rate is increased to $\bar{\gamma}=1$. At the intermediate value of the coupling parameter, $\Gamma=50$ (which is near the value where the minimum of η occurs), the decrease of the viscosity is less significant; it is only $\approx 20\%$. The homogeneous shear algorithm makes it possible to study the contribution of the kinetic and potential parts to the viscosity [the HSA makes use of Eq. (5) in Eq. (13); in Eq. (5), the first term corresponds to the kinetic part while the second term corresponds to the potential part]. Figure 6(b) shows the contributions of the kinetic and potential parts to the viscosity. As can be expected, at the lowest Γ value the kinetic part dominates, while the opposite is found at $\Gamma=300$, which is

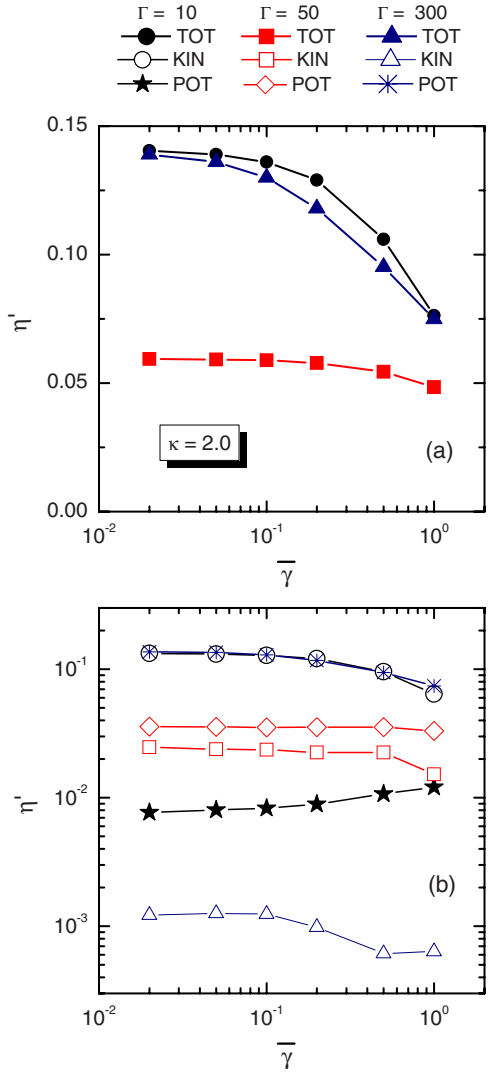

FIG. 6. (Color online) (a) Dependence of the ("TOT") shear viscosity on the normalized shear rate $\bar{\gamma}$ as obtained from HSA calculations, at $\Gamma=10$, 50, and 300, $\kappa=2$. (b) Potential ("POT") and kinetic ("KIN") contributions of the viscosity.

quite close to the solidification point. It is clear that the behavior of the dominant terms is responsible to the overall effect of the applied shear rate on the viscosity. It is interesting to note, however, that a small positive slope shows up in the potential part at $\Gamma=10$, which is overcompensated by the more significant decay of the kinetic contribution. At $\Gamma=50$, the slight decrease of the viscosity is mainly due to the behavior of the kinetic part.

In order to examine the validity of the Stokes-Einstein relation $D\eta/T\cong$const, we take the values of the self-diffusion coefficient from Ohta and Hamaguchi [39]. As the Γ values for which simulation data are available in [39] do not exactly match those for which the (present) viscosity data have been derived, we use Eq. (6) of [39], which gives a functional dependence between the reduced self-diffusion coefficient $D^*=D/\omega_E a^2$ and the normalized temprature $T^*=T/T_m$, where T_m is the melting temperature. Using the present (reference) viscosity data shown in Figs. 3–5, the values of $D^*\eta^*/T^*$ are shown in Fig. 7 as a function of the

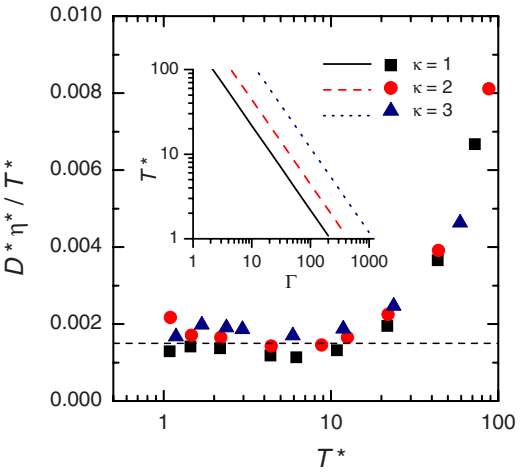

FIG. 7. (Color online) $D^*\eta^*/T^*$ as a function of normalized temperature of the system T^*. The proximity of the data points to the horizontal dashed line indicates the fulfillment of the Stokes-Einstein relation in the $T^*\lesssim 12$ domain. The inset shows the connection between T^* and Γ for the different κ values studied.

normalized temperature T^*. The data points for all the κ values studied lie near a horizontal line at temperatures $T^*\lesssim 12$, implying the Stokes-Einstein relation is fulfilled within a wide domain of temperatures. We do not find a violation of this relation near the solidification point ($T^*=1$), unlike for the 2D system in [30]. At high (normalized) temperatures, the numerical data for $D^*\eta^*/T^*$ deviate significantly from the constant value. If we assume that the universal relationship (i.e., that the deviation from Stokes-Einstein relation depends on the *normalized* temperature) also holds in the Coulomb case, then the fulfillment of the relation would be restricted to $\Gamma\gtrsim 15$. Figure 3(a) of [11] indeed indicates a significant deviation from the Stokes-Einstein relation at $\Gamma\lesssim 20$ in the 3D Coulomb case.

IV. SUMMARY

We have carried out nonequilibrium molecular-dynamics calculations of the shear viscosity (η) of strongly coupled three-dimensional Yukawa liquids. Viscosity values have been obtained for a wide range of the plasma coupling (Γ) and screening (κ) parameters, based on the reverse molecular-dynamics (RMD) method and the homogeneous shear algorithm (HSA). We have studied the influence of the system size on the resulting η values for both techniques. In this respect, the HSA has proven to be superior to the RMD method, as the latter involves a finite length scale and consequently, at lower Γ values where the characteristic distance for momentum transfer becomes comparable with this length, the determinaton of η gets less accurate. In the case of the HSA, the effect of the imposed shear rate on the resulting viscosity values was also checked: no significant differences have been found between the results obtained with $\bar{\gamma}=0.02$ and 0.05. The data obtained with the HSA at $\bar{\gamma}=0.05$ on a system of $N=8000$ particles have been assigned as reference data. (The measured P^{xy} was more noisy in the case of $\bar{\gamma}=0.02$.)

Comparison of the data obtained with the different methods, different system sizes, and shear rates with the reference data showed deviations less than 5% for most of the values. Considering the check for the reproducibility of the results, the accuracy of our reference data can be safely stated to be better than $\pm 5\%$. The viscosity values obtained in previous studies [15,20] appear to scatter randomly around our data [as visible in panels (b) of Figs. 3–5]; no systematic under-or overestimation of η by either of these previous calculations is visible. This suggests that the previous values have indeed larger statistical errors.

Similarly to its 2D counterpart, the 3D Yukawa liquid has been found to be susceptible to shear thinning at high shear rates as seen from the results obtained by the HSA method.

The Stokes-Einstein relation was found to be approximately fulfilled at high coupling values, spanning about an order of magnitude of Γ, bound from above by the value corresponding to the solid-liquid transition. Our results obtained for $D^*\eta^*/T^*$ (using D^* data of [39]) demonstrated that deviation from the Stokes-Einstein relation is governed by the reduced temperature of the system T^*.

Finally, we note that in our calculations, we considered "idealized" Yukawa liquids without any friction and random forces acting on the particles. Simulations for the determination of the shear viscosity considering Langevin dynamics (accounting for the effects of the gas and plasma background) have also been reported recently [40,41]. The methods used in our present work are readily applicable to this approach, and such calculations are planned for future work.

ACKNOWLEDGMENTS

This work has been supported by the Hungarian Fund for Scientific Research through Grant No. OTKA-T-48389, No. OTKA-IN-69892, and No. OTKA-PD-04999. The authors thank Michael Murillo for discussions and Sorin Bastea for providing numerical values of the OCP shear viscosity appearing in Fig. 1 of [19].

[1] *Strongly Coupled Coulomb Systems*, edited by G. J. Kalman, K. B. Blagoev, and M. Rommel (Plenum, New York, 1998).
[2] A. Melzer, V. A. Schweigert, I. V. Schweigert, A. Homann, S. Peters, and A. Piel, Phys. Rev. E **54**, R46 (1996).
[3] J. B. Pieper, J. Goree, and R. A. Quinn, J. Vac. Sci. Technol. A **14**, 519 (1996).
[4] M. Zuzic, A. V. Ivlev, J. Goree, G. E. Morfill, H. M. Thomas, H. Rothermel, U. Konopka, R. Sutterlin, and D. D. Goldbeck, Phys. Rev. Lett. **85**, 4064 (2000).
[5] S. Robertson, A. A. S. Gulbis, J. Collwell, and M. Horányi, Phys. Plasmas **10**, 3874 (2003).
[6] Z. Sternovsky, M. Lampe, and S. Robertson, IEEE Trans. Plasma Sci. **32**, 632 (2004).
[7] H. Löwen, J.-P. Hansen, and J.-N. Roux, Phys. Rev. A **44**, 1169 (1991).
[8] H. Löwen, E. Allahyarov, C. N. Likos, R. Blaak, J. Dzubiella, A. Jusufi, N. Hoffmann, and H. M. Harreis, J. Phys. A **36**, 5827 (2003).
[9] S. Auer and D. Frenkel, J. Phys.: Condens. Matter **14**, 7667 (2002).
[10] A. P. Hynninen and M. Dijkstra, J. Phys.: Condens. Matter **15**, S3557 (2003).
[11] J. Daligault, Phys. Rev. Lett. **96**, 065003 (2006).
[12] G. S. Stringfellow, H. E. DeWitt, and W. L. Slattery, Phys. Rev. A **41**, 1105 (1990).
[13] S. Hamaguchi, R. T. Farouki, and D. H. E. Dubin, Phys. Rev. E **56**, 4671 (1997).
[14] P. Vieillefosse and J. P. Hansen, Phys. Rev. A **12**, 1106 (1975).
[15] T. Saigo and S. Hamaguchi, Phys. Plasmas **9**, 1210 (2002).
[16] J. Wallenborn and M. Baus, Phys. Lett. **61A**, 35 (1977); Phys. Rev. A **18**, 1737 (1978).
[17] B. Bernu, P. Vieillefosse, and J. P. Hansen, Phys. Lett. **63A**, 301 (1977); B. Bernu and P. Vieillefosse, Phys. Rev. A **18**, 2345 (1978).
[18] Z. Donkó and B. Nyíri, Phys. Plasmas **7**, 45 (2000).
[19] S. Bastea, Phys. Rev. E **71**, 056405 (2005).
[20] G. Salin and J.-M. Caillol, Phys. Rev. Lett. **88**, 065002 (2002); Phys. Plasmas **10**, 1220 (2003).
[21] P. Bakshi, Z. Donkó, and G. J. Kalman, Contrib. Plasma Phys. **43**, 261 (2003).
[22] M. S. Murillo, Phys. Rev. E **62**, 4115 (2000).
[23] G. Faussurier and M. S. Murillo, Phys. Rev. E **67**, 046404 (2003).
[24] K. Y. Sanbonmatsu and M. S. Murillo, Phys. Rev. Lett. **86**, 1215 (2001).
[25] M. S. Murillo, High Energy Density Phys. **4**, 49 (2008).
[26] C. L. Chan, W. Y. Woon, and I. L., Phys. Rev. Lett. **93**, 220602 (2004).
[27] A. V. Ivlev, V. Steinberg, R. Kompaneets, H. Höfner, I. Sidorenko, and G. E. Morfill, Phys. Rev. Lett. **98**, 145003 (2007).
[28] Z. Donkó, J. Goree, P. Hartmann, and K. Kutasi, Phys. Rev. Lett. **96**, 145003 (2006).
[29] A. Einstein, Ann. Phys. **322**, 549 (1905).
[30] Bin Liu, J. Goree, and O. S. Vaulina, Phys. Rev. Lett. **96**, 015005 (2006).
[31] O. S. Vaulina, O. F. Petrov, A. V. Gavrikov, X. G. Adamovich, and V. E. Fortov, Phys. Lett. A **372**, 1096 (2008).
[32] O. S. Vaulina and I. E. Dranzhevski, Phys. Scr. **73**, 577 (2006).
[33] J.-P. Hansen and I. R. McDonald, *Theory of Simple Liquids* (Academic, New York, 1976).
[34] F. Müller-Plathe, Phys. Rev. E **59**, 4894 (1999).
[35] D. J. Evans and G. P. Morriss, *Statistical Mechanics of Nonequilibrium Liquids* (Academic, London, 1990).
[36] G. Pan, J. F. Ely, C. McCabe, and D. J. Isbister, J. Chem. Phys. **122**, 094114 (2005).
[37] R. W. Hockney and J. W. Eastwood, *Computer Simulation Using Particles* (McGraw-Hill, 1981).
[38] R. D. Mountain, J. Chem. Phys. **124**, 104109 (2006).
[39] H. Ohta and S. Hamaguchi, Phys. Plasmas **7**, 4506 (2000).
[40] T. S. Ramazanov, K. N. Dzhumagulova, O. F. Petrov, and A. V. Gavrikov, Proceeding of the 33rd EPS Conference on Plasma Physics, Rome, 2006 ECA Vol. 30I, P-4.031 (European Physical Society, Mulhouse, 2006).
[41] T. S. Ramazanov and K. N. Dzhumagulova, Contrib. Plasma Phys. **48**, 357 (2008).